Acta Mech 221, 297–308 (2011)
DOI 10.1007/s00707-011-0506-y

Fei-Xiang Feng · Kang Yong Lee · Yong-Dong Li

Multiple cracks on the interface between a piezoelectric layer and an orthotropic substrate

Received: 6 October 2010 / Published online: 23 June 2011

Abstract In the present work, we investigate the problem of multiple cracks on the interface between a piezoelectric layer and an orthotropic substrate. The method of dislocation simulation and singular integral equation are used to solve the crack problem. The theoretical derivation is verified by the classical result in a special case. Numerical results of the stress intensity factor are obtained, and thereby the effects of geometrical parameters and material orthotropy are surveyed. The optimal stiffness ratio of the orthotropic substrate is suggested for the purpose of interfacial fracture prevention, which is significant for the design and assessment of such a kind of smart structures.

1 Introduction

Artificial piezoelectric ceramics generally act as the kernel components to transfer energy or signals between electro-elastic fields in modern smart devices. To gain advanced performance, piezoelectric components are often made as layered structures. The simplest structure is just composed of a piezoelectric layer and a substrate [1]. Orthotropic polythene composites are sometimes used as the substrate of layered piezoelectric devices to enhance its mechanical performance. In these piezoelectric composites, the interface is an important part that is responsible for the transmission of electro-elastic fields between the layer and the substrate. However, the interface is simultaneously a region that has high stress concentration and thus is subjected to cracking especially when the smart device serves under harsh in situ conditions. Therefore, the problems of interfacial cracks in layered piezoelectric structures have been a focus of the mechanics of piezoelectricity in the past years.

Ru [2] derived the exact elementary solution for interfacial cracks between the embedded electrode layer and piezoelectric ceramic and demonstrated that the electro-elastic fields exhibit power singularities without oscillation. Govorukha and Loboda [3] studied the tensile cracking problem of the interface between a piezoelectric semi-infinite space and a rigid conductor by the method of contact zone model.

F.-X. Feng · Y.-D. Li
Academy of Armored Force Engineering, Beijing 100072, China
E-mail: fengfx@yahoo.com.cn

Y.-D. Li
E-mail: LYDbeijing@163.com

K. Y. Lee (✉)
School of Mechanical Engineering, Yonsei University, Seoul 120-749, Republic of Korea
E-mail: KYL2813@yonsei.ac.kr
Tel.: +82-2-2123-2813
Fax: +82-2-2123-2813

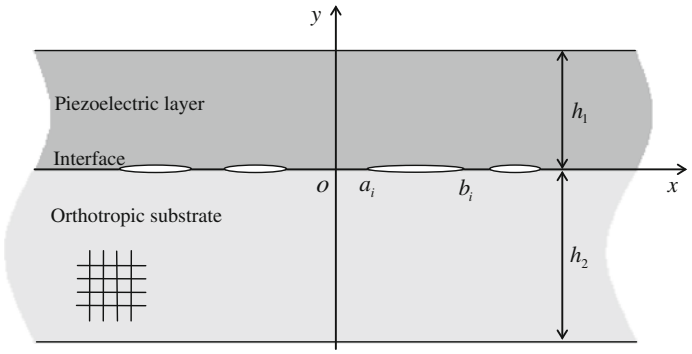

Fig. 1 Multiple interfacial cracks between an orthotropic substrate and a piezoelectric layer

Gu et al. [4] investigated the problem of an interfacial crack between two dissimilar piezoelectric layers under mechanical impacts. Guo and Fang [5] developed an effective simulation method for the problem of interfacial cracking in piezoelectric layers. Huang and Wang [6] surveyed the dynamic behavior of interacting interfacial cracks between a piezoelectric layer and an elastic substrate. Li and Chen [7] performed numerical analysis of interfacial crack tip singularities and the crack tip energy release rates for a permeable interfacial crack in elastic dielectric/piezoelectric bimaterials. Tian and Rajapakse [8] analyzed the fracture parameters of a penny-shaped crack at the interface of a piezoelectric bimaterial system and discussed their dependence on the material properties, poling orientation, and electric loading. Li and Lee [9] performed fracture analysis on the arc-shaped interface in a layered cylindrical piezoelectric sensor polarized along its axis by the methods of infinite series and singular integral equation. Hausler et al. [10] examined the fracture behavior of metal–piezoceramic interfaces under mechanical and electrical loading by experiments. Shin and Lee [11] studied the dynamic propagation of an interfacial crack between two dissimilar functionally graded piezoelectric layers under electromechanical loading. Loboda et al. [12] investigated the in-plane fracture of a thin isotropic interlayer sandwiched between two identical piezoelectric semi-infinite spaces by considering the zones of electrical saturation and mechanical yielding. Natroshvili et al. [13] addressed the three-dimensional interfacial crack problems for metallic-piezoelectric composite bodies and discussed the dependence of the stress singularity exponents on the material parameters.

Sometimes, the elastic substrates may be reinforced by fibers orthogonally to enhance the performances of piezoelectric composites. Therefore, investigation on the fracture behavior of piezoelectric composites with orthotropic substrates has practical significance. However, only few work has been done in this field. Kwon and Meguid [14] provided the analytical solution for a central crack normal to a piezoelectric–orthotropic interface. Kwon and Lee [15] studied the dynamic propagation of an eccentric crack in a piezoelectric layer bonded between two orthotropic elastic layers under the combined anti-plane mechanical shear and in-plane electrical loadings. To our knowledge, none has considered the interfacial fracture problems of piezoelectric composites with orthotropic substrates. In the present work, the problem of multiple cracks on the interface between a piezoelectric layer and an orthotropic substrate is solved by the method of dislocation simulation and singular integral equation [16–18]. Numerical results of the stress intensity factor are obtained, and the effects of geometrical parameters and stiffness ratio are revealed, which may provide references for the design and assessment of this kind of smart structures.

2 Problem formulation

Illustrated in Fig. 1 is a composite composed of a piezoelectric layer and an orthotropic substrate. The thickness of the former is h_1 and that of the latter is h_2. The rectangular coordinate system is established with the rightward x axis along the interface and the upward y axis along the thickness direction. There are multiple cracks on the interface, occupying the intervals, $x \in (a_i, b_i)$, $(i = 1, 2, \ldots, n)$, respectively. The piezoelectric layer is poled along the z axis and isotropic in the xoy plane.

Assume that the upper and lower surfaces of the composite are free of loading and only the surfaces of the cracks are loaded by equivalent anti-plane shear traction $-\tau_0$. The boundary and continuity conditions of the problem take the form

$$\tau_{yz}^{(1)}(x, h_1) = 0; \quad \tau_{yz}^{(2)}(x, -h_2) = 0, \tag{1}$$

$$D_y^{(1)}(x, h_1) = 0; \quad D_y^{(1)}(x, 0) = 0, \tag{2}$$

$$\tau_{yz}^{(1)}(x, +0) = \tau_{yz}^{(2)}(x, -0), \quad x \notin (a_i, b_i), \quad i = 1, 2, \ldots, n, \tag{3}$$

$$w_1(x, +0) = w_2(x, -0), \quad x \notin (a_i, b_i), \quad i = 1, 2, \ldots, n, \tag{4}$$

$$\tau_{yz}^{(1)}(x, +0) = \tau_{yz}^{(2)}(x, -0) = -\tau_0, \quad x \in (a_i, b_i), \quad i = 1, 2, \ldots, n, \tag{5}$$

where w and τ denote the mechanical displacement and stress. D is the electric displacement. The superscripts/subscripts 1 and 2 refer to the quantities of the piezoelectric layer and orthotropic substrate, respectively.

3 Fracture analysis

3.1 Fields induced by point dislocation

A convenient way to treat the problem of collinear cracks is to simulate them by continuously distributed dislocations [17,18], whose density functions are defined by

$$g_i(x) = \frac{\mathrm{d}}{\mathrm{d}x}\left[w_1^{(i)}(x, 0) - w_2^{(i)}(x, 0)\right], \quad (i = 1, 2, \ldots, n). \tag{6}$$

According to Eq. (4) and the dislocation-based theory of fracture mechanics, dislocation density functions should satisfy the following single-valuedness conditions [19]:

$$\int_{a_i}^{b_i} g_i(t)\,\mathrm{d}t = 0, \quad (i = 1, 2, \ldots, n). \tag{7}$$

The solution of continuously distributed dislocations may be obtained by integrating that of a point dislocation. A point dislocation placed on the interface is described by

$$\frac{\mathrm{d}}{\mathrm{d}x}[w_1(x, 0) - w_2(x, 0)] = \delta(x - s), \tag{8}$$

where s is the x coordinate of the point dislocation. δ is the Dirac delta function.

Separate the Dirac delta function $\delta(x - s)$ into even and odd parts [17,18]. Then, Eq. (8) becomes

$$\frac{\mathrm{d}}{\mathrm{d}x}[w_1(x, 0) - w_2(x, 0)] = \frac{1}{2}[\omega(x) + \lambda(x)], \tag{9}$$

where

$$\left.\begin{aligned} \omega(x) &= \delta(x + s) + \delta(x - s) \\ \lambda(x) &= \delta(x - s) - \delta(x + s) \end{aligned}\right\} \tag{10}$$

Next, we use the method of Fourier transform to get the electric/elastic field induced by the point dislocation. The basic equations of the piezoelectric layer read [20]

$$\left.\begin{aligned} \tau_{kz}^{(1)} &= c_{44}^{(1)}\frac{\partial w_1}{\partial k} + e_{15}\frac{\partial \phi}{\partial k} \\ D_k &= e_{15}\frac{\partial w_1}{\partial k} - \varepsilon_{11}\frac{\partial \phi}{\partial k} \end{aligned}\right\}, k = x, y, \tag{11}$$

$$\frac{\partial \tau_{xz}^{(1)}}{\partial x} + \frac{\partial \tau_{yz}^{(1)}}{\partial y} = 0; \frac{\partial D_x}{\partial x} + \frac{\partial D_y}{\partial y} = 0, \tag{12}$$

where ϕ is the electric potential. $c_{44}^{(1)}$, e_{15} and ε_{11} are the elastic constant, piezoelectric coefficient, and dielectric coefficient.

Generally, it is reasonable to assume that $c_{44}^{(1)}\varepsilon_{11} + e_{15}^2 \neq 0$. So, substituting Eq. (11) into Eq. (12) yields

$$\left.\begin{aligned} \nabla^2 w_1(x, y) &= 0 \\ \nabla^2 \phi(x, y) &= 0 \end{aligned}\right\} \tag{13}$$

where ∇^2 is the Laplacian operator.

The basic equations of the orthotropic substrate are

$$\tau_{zx}^{(2)} = c_{55}^{(2)} \frac{\partial w_2}{\partial x}; \tau_{zy}^{(2)} = c_{44}^{(2)} \frac{\partial w_2}{\partial y}, \tag{14}$$

$$\frac{\partial \tau_{zx}^{(2)}}{\partial x} + \frac{\partial \tau_{zy}^{(2)}}{\partial y} = 0, \tag{15}$$

where $c_{44}^{(2)}$ and $c_{55}^{(2)}$ are two elastic constants.

Substituting Eq. (14) into Eq. (15) gives

$$\alpha^2 \frac{\partial^2 w_2}{\partial x^2} + \frac{\partial^2 w_2}{\partial y^2} = 0, \tag{16}$$

where $\alpha = \sqrt{c_{55}^{(2)}/c_{44}^{(2)}}$.

It deserves noting that $\omega(x)$ is an even function but $\lambda(x)$ is an odd function. Therefore, the electric/elastic field induced by $\omega(x)/2$ has symmetry with respect to the y axis, but that by $\lambda(x)/2$ has anti-symmetry instead.

Applying Fourier transform to Eqs. (13) and (16) with respect to x, one can obtain the electric/elastic field produced by $\omega(x)/2$:

$$\left.\begin{aligned} w_1^{(\omega)}(x,y) &= \tfrac{2}{\pi}\int_0^{+\infty}\left[A_1(\xi)e^{-\xi y} + A_2(\xi)e^{\xi y}\right]\cos(\xi x)\mathrm{d}\xi \\ \phi_\omega(x,y) &= \tfrac{2}{\pi}\int_0^{+\infty}\left[A_5(\xi)e^{-\xi y} + A_6(\xi)e^{\xi y}\right]\cos(\xi x)\mathrm{d}\xi \end{aligned}\right\} \tag{17}$$

$$w_2^{(\omega)}(x,y) = \frac{2}{\pi}\int_0^{+\infty}\left[A_9(\xi)e^{-\alpha\xi y} + A_{10}(\xi)e^{\alpha\xi y}\right]\cos(\xi x)\mathrm{d}\xi. \tag{18}$$

Also by Fourier transform, the electric/elastic field produced by $\lambda(x)/2$ may be obtained:

$$\left.\begin{aligned} w_1^{(\lambda)}(x,y) &= \tfrac{2}{\pi}\int_0^{+\infty}\left[A_3(\xi)e^{-\xi y} + A_4(\xi)e^{\xi y}\right]\sin(\xi x)\mathrm{d}\xi \\ \phi_\lambda(x,y) &= \tfrac{2}{\pi}\int_0^{+\infty}\left[A_7(\xi)e^{-\xi y} + A_8(\xi)e^{\xi y}\right]\sin(\xi x)\mathrm{d}\xi \end{aligned}\right\} \tag{19}$$

$$w_2^{(\lambda)}(x,y) = \frac{2}{\pi}\int_0^{+\infty}\left[A_{11}(\xi)e^{-\alpha\xi y} + A_{12}(\xi)e^{\alpha\xi y}\right]\sin(\xi x)\mathrm{d}\xi. \tag{20}$$

In Eqs. (17)–(20), $A_j(\xi)$ $(j = 1, 2, \ldots, 12)$ are undetermined coefficient functions. Referring to Eqs. (8) and (9), one may obtain the electric/elastic field produced by the point dislocation

$$\left.\begin{aligned} w_1(x,y) &= \tfrac{2}{\pi}\int_0^{+\infty}\left(A_1e^{-\xi y} + A_2e^{\xi y}\right)\cos(\xi x)\mathrm{d}\xi \\ &\quad + \tfrac{2}{\pi}\int_0^{+\infty}\left(A_3e^{-\xi y} + A_4e^{\xi y}\right)\sin(\xi x)\mathrm{d}\xi \\ \phi(x,y) &= \tfrac{2}{\pi}\int_0^{+\infty}\left(A_5e^{-\xi y} + A_6e^{\xi y}\right)\cos(\xi x)\mathrm{d}\xi \\ &\quad + \tfrac{2}{\pi}\int_0^{+\infty}\left(A_7e^{-\xi y} + A_8e^{\xi y}\right)\sin(\xi x)\mathrm{d}\xi \end{aligned}\right\} \tag{21}$$

$$w_2(x,y)=\frac{2}{\pi}\int_0^{+\infty}\left(A_9e^{-\alpha\xi y}+A_{10}e^{\alpha\xi y}\right)\cos(\xi x)\mathrm{d}\xi$$
$$+\frac{2}{\pi}\int_0^{+\infty}\left(A_{11}e^{-\alpha\xi y}+A_{12}e^{\alpha\xi y}\right)\sin(\xi x)\mathrm{d}\xi. \tag{22}$$

It follows from Eqs. (21), (22), (11), and (14) that

$$\tau_{yz}^{(1)}(x,y)=\frac{2}{\pi}\int_0^{+\infty}\left[c_{44}^{(1)}\left(A_2e^{\xi y}-A_1e^{-\xi y}\right)+e_{15}\left(A_6e^{\xi y}-A_5e^{-\xi y}\right)\right]\xi\cos(\xi x)\mathrm{d}\xi$$
$$+\frac{2}{\pi}\int_0^{+\infty}\left[c_{44}^{(1)}\left(A_4e^{\xi y}-A_3e^{-\xi y}\right)+e_{15}\left(A_8e^{\xi y}-A_7e^{-\xi y}\right)\right]\xi\sin(\xi x)\mathrm{d}\xi, \tag{23}$$

$$D_y(x,y)=\frac{2}{\pi}\int_0^{+\infty}\left[e_{15}\left(A_2e^{\xi y}-A_1e^{-\xi y}\right)-\varepsilon_{11}\left(A_6e^{\xi y}-A_5e^{-\xi y}\right)\right]\xi\cos(\xi x)\mathrm{d}\xi$$
$$+\frac{2}{\pi}\int_0^{+\infty}\left[e_{15}\left(A_4e^{\xi y}-A_3e^{-\xi y}\right)-\varepsilon_{11}\left(A_8e^{\xi y}-A_7e^{-\xi y}\right)\right]\xi\sin(\xi x)\mathrm{d}\xi, \tag{24}$$

$$\tau_{zy}^{(2)}(x,y)=c_{44}^{(2)}\frac{2}{\pi}\int_0^{+\infty}\left(A_{10}e^{\alpha\xi y}-A_9e^{-\alpha\xi y}\right)\alpha\xi\cos(\xi x)\mathrm{d}\xi$$
$$+c_{44}^{(2)}\frac{2}{\pi}\int_0^{+\infty}\left(A_{12}e^{\alpha\xi y}-A_{11}e^{-\alpha\xi y}\right)\alpha\xi\sin(\xi x)\mathrm{d}\xi. \tag{25}$$

Using Eqs. (21)–(25), one may transform Eqs. (1)–(3) and (9) into integral equations. Separating their even and odd parts with respect to x and then applying cosine and sine transforms accordingly yield a system of algebraic equations. The coefficient matrix $\mathbf{M}$ of these algebraic equations is given in the Appendix. Solving these algebraic equations gives

$$A_j(\xi)=[\beta_{j1}(\xi)\cos(\xi s)-\beta_{j2}(\xi)\sin(\xi s)]/(2\xi),\quad (j=1,\ 2,\ \ldots,\ 12), \tag{26}$$

where $\beta_{j1}(\xi)$ and $\beta_{j2}(\xi)$ $(j=1,\ 2,\ \ldots,\ 12)$ are the first and second columns of elements of $\mathbf{M}^{-1}$. Here, the superscript -1 represents the inverse matrix.

Substituting Eq. (26) into Eq. (25) leads to

$$\tau_{yz}(x,0)=\sqrt{c_{44}^{(2)}c_{55}^{(2)}}\frac{1}{\pi}\int_0^{+\infty}[Q_1(\xi)\sin(\xi s)+Q_3(\xi)\cos(\xi s)]\cos(\xi x)\mathrm{d}\xi$$
$$+\sqrt{c_{44}^{(2)}c_{55}^{(2)}}\frac{1}{\pi}\int_0^{+\infty}[Q_2(\xi)\cos(\xi s)+Q_4(\xi)\sin(\xi s)]\sin(\xi x)\mathrm{d}\xi, \tag{27}$$

where $Q_1,\ Q_2,\ Q_3$ and Q_4 are four dimensionless functions defined by

$$\left.\begin{array}{ll}Q_1(\xi)=\beta_{92}(\xi)-\beta_{(10)2}(\xi); & Q_3(\xi)=\beta_{(10)1}(\xi)-\beta_{91}(\xi)\equiv 0\\ Q_2(\xi)=\beta_{(12)1}(\xi)-\beta_{(11)1}(\xi); & Q_4(\xi)=\beta_{(11)2}(\xi)-\beta_{(12)2}(\xi)\equiv 0\end{array}\right\} \tag{28}$$

When $\xi\to\infty$, the asymptotic values of Q_1 and Q_2 are

$$\lim_{\xi\to\infty}Q_1(\xi)=-\lim_{\xi\to\infty}Q_2(\xi)=q\neq 0, \tag{29}$$

where q is a dimensionless constant given by

$$q = \frac{c_{44}^{(1)}\varepsilon_{11} + e_{15}^2}{c_{44}^{(1)}\varepsilon_{11} + e_{15}^2 + \alpha c_{44}^{(2)}\varepsilon_{11}}. \tag{30}$$

Considering Eqs. (28) and (29), one can reformulate Eq. (27) into

$$\tau_{yz}(x,0) = \sqrt{c_{44}^{(2)}c_{55}^{(2)}}\frac{1}{\pi}\left[\frac{q}{s-x} + R(s,x)\right], \tag{31}$$

where $R(s,x)$ is a function defined by

$$\begin{aligned} R(s,x) = &\int_0^{+\infty} [Q_1(\xi) - q]\sin(\xi s)\cos(\xi x)\mathrm{d}\xi \\ &+ \int_0^{+\infty} [Q_2(\xi) + q]\cos(\xi s)\sin(\xi x)\mathrm{d}\xi. \end{aligned} \tag{32}$$

In the derivation of Eq. (32), the following integral formula is used [21]:

$$\int_0^{\infty} \sin(\xi s)\cos(\xi x)\mathrm{d}\xi = \frac{1}{2}\left(\frac{1}{s+x} + \frac{1}{s-x}\right). \tag{33}$$

Equation (31) gives the stress $\tau_{yz}(x,0)$ on the interface induced by a point dislocation placed at $x = s$ on the x axis.

As indicated by Eq. (6), the multiple cracks on the interface in Fig. 1 can be simulated by dislocations continuously distributed in the intervals, $x \in (a_i,\ b_i)$, $(i = 1,\ 2,\ \ldots,\ n)$, respectively. According to the theory of Green's function and the principle of superposition, the stress $\tau_{yz}(x,0)$ induced by these continuously distributed dislocations can be formulated as

$$\tau_{yz}(x,0) = \sqrt{c_{44}^{(2)}c_{55}^{(2)}}\frac{1}{\pi}\sum_{j=1}^{n}\int_{a_j}^{b_j} g_j(s)\left[\frac{q}{s-x} + R(s,x)\right]\mathrm{d}s. \tag{34}$$

3.2 Singular integral equation

Substituting Eq. (34) into Eq. (5) gives

$$\frac{1}{\pi}\sum_{j=1}^{n}\int_{a_j}^{b_j} g_j(s_j)\left[\frac{1}{s_j - x_k} + q^{-1}R(s_j,x_k)\right]\mathrm{d}s_j = \frac{-\tau_0}{q\sqrt{c_{44}^{(2)}c_{55}^{(2)}}},\ x_k \in (a_k,\ b_k), \tag{35}$$

where $k = 1,\ 2,\ \ldots,\ n$. Obviously, only when $s_j = x_k$ would the integral associated with $(s_j - x_k)^{-1}$ have the Cauchy type singularity.

For the convenience of numerical computation, let's introduce the following dimensionless quantities

$$\left.\begin{aligned} \tilde{s}_j &= (s_j - c_{0j})/a_{0j} \in (-1,\ 1) \\ \tilde{x}_j &= (x_j - c_{0j})/a_{0j} \in (-1,\ 1) \end{aligned}\right\},\quad (j = 1,\ 2,\ \ldots,\ n), \tag{36}$$

where $a_{0j} = (b_j - a_j)/2$ is the half-length of the jth crack and $c_{0j} = (b_j + a_j)/2$ is the x coordinate of its center.

Using Eq. (36), one can recast Eq. (35) into standard form:

$$\sum_{j=1}^{n}\frac{1}{\pi}\int_{-1}^{1}\tilde{g}_j(\tilde{s}_j)\left[\frac{a_{0j}}{a_{0j}\tilde{s}_j+c_{0j}-a_{0k}\tilde{x}_k-c_{0k}}+\tilde{R}(\tilde{s}_j,\tilde{x}_k)\right]\mathrm{d}\tilde{s}_j=\frac{-\tau_0}{q\sqrt{c_{44}^{(2)}c_{55}^{(2)}}},\tag{37}$$

where $k=1,\ 2,\ \ldots,\ n$ and

$$\left.\begin{aligned}\tilde{R}(\tilde{s}_j,\tilde{x}_k)&=a_{0j}q^{-1}R(a_{0j}\tilde{s}_j+c_{0j},\ a_{0k}\tilde{x}_k+c_{0k})\\ \tilde{g}_j(\tilde{s}_j)&=g_j(a_{0j}\tilde{s}_j+c_{0j})\end{aligned}\right\}\tag{38}$$

According to the theory of Cauchy singular integral equation [22], the dislocation density functions $\tilde{g}_j(\tilde{s}_j)$ $(j=1,\ 2,\ldots,\ n)$ in Eq. (37) have the square-root type singularity. Therefore, by introducing undetermined dimensionless non-singular functions $f_j(\tilde{s}_j)$ $(j=1,\ 2,\ \ldots,\ n)$ and separating the singular part, the dislocation density functions may be expressed as

$$\tilde{g}_j(\tilde{s}_j)=\frac{\tau_0}{q\sqrt{c_{44}^{(2)}c_{55}^{(2)}}}\frac{f_j(\tilde{s}_j)}{\sqrt{1-\tilde{s}_j^2}},\quad(j=1,\ 2,\ \ldots,\ n).\tag{39}$$

Then, using the method of Lobatto-Chebyshev quadrature, one can transform Eqs. (37) and (7) into algebraic equations:

$$\sum_{r=0}^{m}\chi_r\sum_{j=1}^{n}f_j(\tilde{s}_{jr})\left[\frac{a_{0j}}{a_{0j}\tilde{s}_{jr}+c_{0j}-a_{0k}\tilde{x}_{kt}-c_{0k}}+\tilde{R}(\tilde{s}_{jr},\tilde{x}_{kt})\right]=-m,\tag{40}$$

$$\sum_{r=0}^{m}\chi_r f_k(\tilde{s}_{kr})=0,\tag{41}$$

where $k=1,\ 2,\ \ldots,\ n;\ t=1,\ 2,\ \ldots,\ m$. m is the node number of the numerical quadrature. χ_i $(i=1,\ 2,\ \ldots,\ m)$ are the weighting coefficients given by $\chi_0=\chi_m=1/2$ and $\chi_1=\cdots=\chi_{m-1}=1$. The discrete values of $\tilde{s}_j$ and $\tilde{x}_k$ are the roots of the Chebyshev polynomials of the first and second kind, respectively:

$$\left.\begin{aligned}\tilde{s}_{jr}&=\cos(r\pi/m)\ ,\quad(r=0,\ 1,\ \ldots,\ m)\\ \tilde{x}_{kt}&=\cos[(2t-1)\pi/(2m)],\quad(t=1,\ 2,\ \ldots,\ m)\end{aligned}\right\}\tag{42}$$

One may solve Eqs. (40) and (41) numerically to get the solutions of $f_j(\tilde{s}_j)$ $(j=1,\ 2,\ \ldots,\ n)$, which can be further used to determine the stress intensity factor (SIF).

3.3 Stress intensity factor

The SIFs of the two tips of every crack is defined by

$$\left.\begin{aligned}K_{ak}&=\lim_{x\to a_k^-}\tau_{yz}(x,\ 0)\sqrt{2\pi(a_k-x)}\\ K_{bk}&=\lim_{x\to b_k^+}\tau_{yz}(x,\ 0)\sqrt{2\pi(x-b_k)}\end{aligned}\right\},\quad(k=1,\ 2,\ \ldots,\ n).\tag{43}$$

According to Eq. (34), the singular part of $\tau_{yz}(x,\ 0)$ is

$$\left.\begin{aligned}\lim_{x_k\to a_k^-}\tau_{yz}(x,0)&=q\sqrt{c_{44}^{(2)}c_{55}^{(2)}}\frac{1}{\pi}\lim_{\tilde{x}_k\to-1^-}\int_{-1}^{1}\frac{\tilde{g}_k(\tilde{s}_k)}{\tilde{s}_k-\tilde{x}_k}\mathrm{d}\tilde{s}_k\\ \lim_{x_k\to b_k^+}\tau_{yz}(x,0)&=q\sqrt{c_{44}^{(2)}c_{55}^{(2)}}\frac{1}{\pi}\lim_{\tilde{x}_k\to1^+}\int_{-1}^{1}\frac{\tilde{g}_k(\tilde{s}_k)}{\tilde{s}_k-\tilde{x}_k}\mathrm{d}\tilde{s}_k\end{aligned}\right\}\tag{44}$$

where $k=1,\ 2,\ \ldots,\ n$.

Substituting Eq. (39) into Eq. (44), one may rewrite the singular part of $\tau_{yz}(x,\ 0)$ as [23]

$$\left.\begin{array}{l}\lim\limits_{x_k\to a_k^-}\tau_{yz}(x,0)=\tau_0\lim\limits_{\tilde{x}_k\to -1^-}\frac{f_k(-1)}{\sqrt{\tilde{x}_k^2-1}}\\ \lim\limits_{x_k\to b_k^+}\tau_{yz}(x,0)=\tau_0\lim\limits_{\tilde{x}_k\to 1^+}\frac{-f_k(1)}{\sqrt{\tilde{x}_k^2-1}}\end{array}\right\},(k=1,\ 2,\ \ldots,\ n). \tag{45}$$

In the derivation of Eq. (45), the following integral formula is used [24]:

$$\frac{1}{\pi}\int_{-1}^{1}\frac{1}{(\tilde{s}-\tilde{x})\sqrt{1-\tilde{s}^2}}\mathrm{d}\tilde{s}=\begin{cases}\frac{-1}{\sqrt{\tilde{x}^2-1}}, & \tilde{x}>1,\\ 0, & |\tilde{x}|<1\\ \frac{1}{\sqrt{\tilde{x}^2-1}}, & \tilde{x}<-1.\end{cases} \tag{46}$$

Substituting Eq. (45) into Eq. (43) yields

$$\left.\begin{array}{l}K_{ak}=\tau_0 f_k(-1)\sqrt{\pi a_{0k}}\\ K_{bk}=-\tau_0 f_k(1)\sqrt{\pi a_{0k}}\end{array}\right\},\quad (k=1,\ 2,\ \ldots,\ n). \tag{47}$$

Because $\tau_0\sqrt{\pi a_{0k}}$ has the dimension of SIF, we can use it to normalize the SIFs in Eq. (47). So, in the numerical computation, we only calculate the following dimensionless SIFs:

$$\left.\begin{array}{l}K_{ak}=f_k(-1)\\ K_{bk}=-f_k(1)\end{array}\right\},\quad (k=1,\ 2,\ \ldots,\ n). \tag{48}$$

3.4 Verification

One can use a special case to verify the foregoing derivation. Assume that $e_{15}=0$, $c_{55}^{(2)}=c_{44}^{(2)}=c_{44}^{(1)}=c_{44}$ and $h_1=h_2\to\infty$; then, the problem in Fig. 1 becomes that of collinear cracks in an elastic isotropic plane. In this special case, we have $\alpha=1$, $q=1/2$ and $\lim\limits_{h_1=h_2\to\infty}R(s,x)=0$. What is more, because the problem is antisymmetric with respect to the x axis, it is sufficient to study only the upper half-plane. Therefore, the dislocation density function can be defined as

$$G_j(x)=\frac{\mathrm{d}}{\mathrm{d}x}w_j(x,\ 0^+)=\frac{1}{2}g_j(x),\quad (j=1,\ 2,\ \ldots,\ n). \tag{49}$$

Then, Eq. (35) reduces to

$$\sum_{j=1}^{n}\frac{1}{\pi}\int_{a_j}^{b_j}\frac{G_j(s_j)}{s_j-x_k}\mathrm{d}s_j=-\frac{\tau_0}{c_{44}},\quad x_k\in(a_k,\ b_k). \tag{50}$$

If there is only one crack lying in the interval $x\in(-a,\ a)$, Eq. (50) further reduces to

$$\frac{1}{\pi}\int_{-a}^{a}\frac{G(s)}{s-x}\mathrm{d}s=-\frac{\tau_0}{c_{44}},\quad x\in(-a,\ a). \tag{51}$$

Equation (51) is the classical singular integral equation for a mode III crack in an elastic isotropic plane. The degradation from Eq. (35) to Eq. (51) validates the foregoing theoretical derivation.

4 Numerical results and discussion

Assume that the piezoelectric layer is PZT-5H ceramic. Its material constants are $c_{44}^{(1)}=3.53\times10^{10}$ N/m^2, $\varepsilon_{11}=151.0\times10^{-10}$ C/(Vm) and $e_{15}=17.0$ C/m^2. The substrate is orthotropic polythene composite, and its elastic constants are $c_{44}^{(2)}=1.765\times10^{10}$ N/m^2 and $c_{55}^{(2)}=\alpha^2c_{44}^{(2)}$. For the convenience of computation, we only consider the special case of two interfacial cracks in this section.

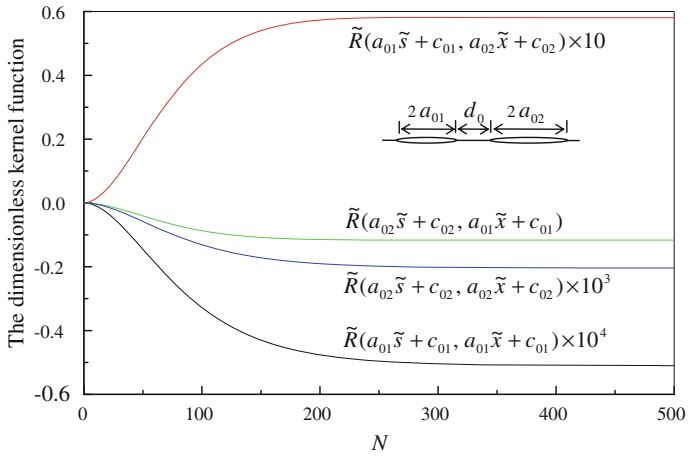

Fig. 2 The asymptotic behaviors of the dimensionless kernel function ($h_1 = h_2 = 10$ mm; $a_{02} = 2a_{01} = 5$ mm; $d_0 = 1$ mm; $c_{44}^{(2)} = 17.65$ GPa; $\alpha = 1.5$)

4.1 Computational accuracy

At the beginning of computation, it is necessary to survey the convergence behavior of the dimensionless non-singular kernel function $\tilde{R}(\tilde{s}_j, \tilde{x}_k)$, $(j = 1,\ 2; k = 1,\ 2)$. As indicated by Eq. (32), this kernel function involves infinite integral. A practical method to quadrature this infinite integral is to truncate it into a finite integral on the interval $(0,\ N)$, where the value of the upper limit N depends on the convergence speed of the integration [23]. Illustrated in Fig. 2 is the variation of the kernel function versus the upper limit N. It is indicated that the kernel function converges very well. $N = 500$ is quite enough to guarantee a precision of 1.0×10^{-6}, which is sufficient for most engineering applications. Therefore, N is fixed at 500 in the following computation.

In addition, the quadrature node number m is another parameter affecting the accuracy of the numerical results. Calculation reveals that $m = 20$ is well enough to ensure a precision of 1.0×10^{-6} with satisfactory computational efficiency.

4.2 Parametric studies

4.2.1 Effect of geometrical parameters

Figure 3 shows the effects of crack space and structure thickness on the SIFs. If the crack space $d_0 \geq 10a_0$, the variation of d_0 nearly does not affect the SIF. As d_0 decreases from $10a_0$ to $5a_0$, the SIF only increases slightly. If d_0 continues to decrease from $5a_0$, the SIF begins to increase notably. When $d_0 \to 0$, the SIFs of the two inner tips even experience a singular increase, which would gives rise to a sudden interlinkage between the two cracks.

It deserves noting that in Fig. 3, the SIFs of the two outer tips also increase as the crack space decreases, although their increase is smaller than that of the two inner tips. This is because the two cracks in Fig. 3 are so short than their outer tips also fall into the affected region of the crack space. Further computation indicates that if the cracks are long enough the variation of the crack space would have a vanishing effect on the SIFs of the outer tips.

Figure 3 also reveals that the interfacial cracks in a structure with smaller thickness would have larger SIFs. This is because the surfaces of a thinner structure affect the interfacial cracks more notably, which leads to the increase in their SIFs. As the half thickness h becomes larger than $10a_0$, the effect of the structure surfaces becomes negligible and the SIFs then get insensitive to the variation of the structure thickness.

4.2.2 Crack opening mouth

It follows from Eq. (6) that we can calculate the dislocation between the crack surfaces by numerical integration after the numerical solution of the dislocation density function is obtained. Figure 4 presents the dislocations

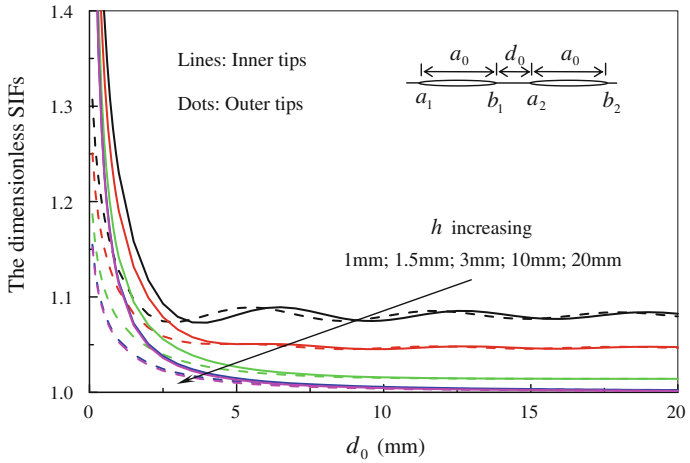

Fig. 3 The effects of crack space and structure thickness on the SIFs ($a_0 = 1$ mm; $h_1 = h_2 = h$; $c_{44}^{(2)} = 17.65$ GPa; $\alpha = 1.5$)

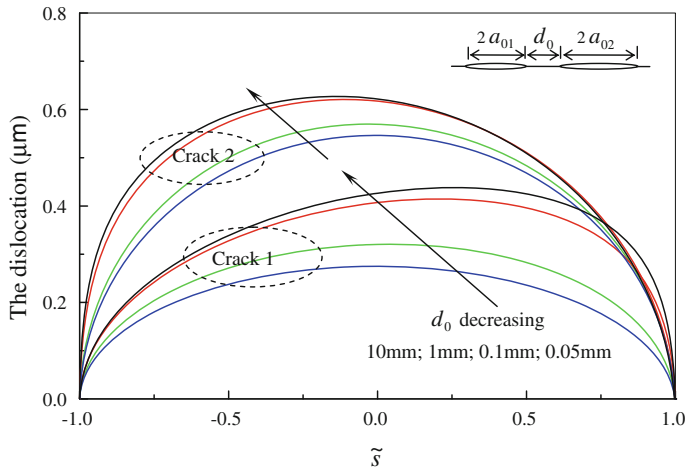

Fig. 4 The dislocations of the cracks ($h_1 = h_2 = 10$ mm; $a_{02} = 2a_{01} = 2$ mm; $\tau_0 = 5$ MPa; $c_{44}^{(2)} = 17.65$ GPa; $\alpha = 1.5$)

of two interfacial cracks when the crack-surface traction is prescribed as $\tau_0 = 5$ MPa. In this figure, $\tilde{s} = -1.0$ corresponds to the inner-side tip of crack 2 and the outer-side tip of crack 1, while $\tilde{s} = 1.0$ to the inner-side tip of crack 1 and the outer-side tip of crack 2. It is revealed that the dislocation curves of both cracks become oblique to the inner side as the crack space d_0 decreases. This is in consistence with the common sense of fracture mechanics.

4.2.3 Effect of orthotropy

Anti-plane deformation of the orthotropic substrate involves two stiffness coefficients, $c_{55}^{(2)}$ and $c_{44}^{(2)}$, and their ratio $c_{55}^{(2)}/c_{44}^{(2)}$ reflects the degree of material orthotropy. In all the foregoing computation, this ratio is fixed (see Figs. 2, 3, 4: $\alpha = 1.5$). This subsection continues to examine the effect of the stiffness ratio $c_{55}^{(2)}/c_{44}^{(2)}$ on the interfacial cracks. Figure 5 shows that as $c_{55}^{(2)}/c_{44}^{(2)}$ decreases from 1.0 to 0.1, the SIFs increase remarkably. However, the SIFs nearly keep unchanged when $c_{55}^{(2)}/c_{44}^{(2)}$ increases from 1.0 to 10.0. This is consistent with the results of some related previous studies. For example, see Figs. 3 and 4 of Matbuly and Nassar [25], and Figs. 7 and 8 of Li and Duan [26]. Therefore, in order to prevent the interfacial fracture, it is better to choose an orthotropic substrate with its stiffness ratio lager than 1.0. If the stiffness ratio of the orthotropic substrate is less than 1.0, the risk of interface fracture would be enhanced.

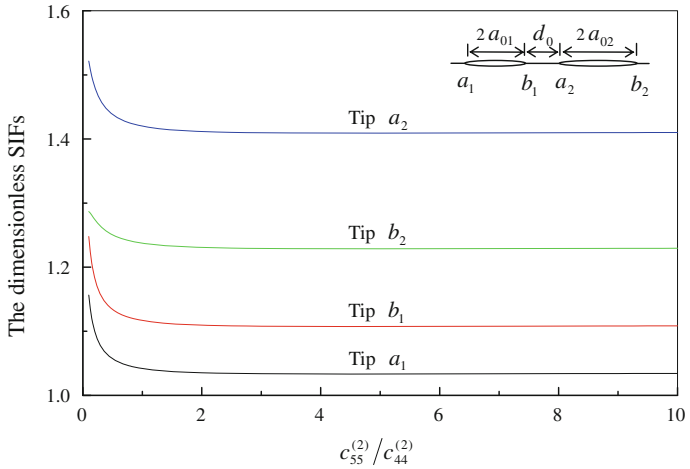

Fig. 5 The effects of $c_{55}^{(2)}/c_{44}^{(2)}$ on the SIFs ($h_1 = h_2 = 10$ mm; $a_{02} = 3$ mm; $a_{01} = 1$ mm; $d_0 = 1$ mm; $c_{44}^{(2)} = 17.65$ GPa)

5 Conclusions

Interfacial fracture is a typical failure of layered piezoelectric composites. Fracture analysis is an important way to assess the safety of the interface and to find some feasible approaches to prevent interfacial fracture. In the present work, Fracture analysis is performed on a smart composite consisting of a piezoelectric layer and an orthotropic substrate with multiple cracks lying on the interface. The cracks are simulated as continuously distributed dislocations, and then the method of singular integral equation is used to solve the problem. The derivation is verified by the classical result in a special case. Numerical results of the stress intensity factor are used to survey the effects of geometrical and physical parameters. The optimal stiffness ratio of the orthotropic substrate is suggested for the purpose of interfacial fracture prevention.

Acknowledgments This work is supported by the BK 21 program of South Korea.

Appendix

The nonvanishing elements of the coefficient matrix M are

$$
\begin{aligned}
&M_{13} = 1;\ M_{14} = 1;\ M_{1(11)} = -1;\ M_{1(12)} = -1;\\
&M_{21} = 1;\ M_{22} = 1;\ M_{29} = -1;\ M_{2(10)} = -1;\\
&M_{31} = -c_{44}^{(1)}\mathrm{e}^{-\xi h_1};\quad M_{32} = c_{44}^{(1)}\mathrm{e}^{\xi h_1};\quad M_{35} = -e_{15}\mathrm{e}^{-\xi h_1};\quad M_{36} = e_{15}\mathrm{e}^{\xi h_1};\\
&M_{43} = -c_{44}^{(1)}\mathrm{e}^{-\xi h_1};\quad M_{44} = c_{44}^{(1)}\mathrm{e}^{\xi h_1};\quad M_{47} = -e_{15}\mathrm{e}^{-\xi h_1};\quad M_{48} = e_{15}\mathrm{e}^{\xi h_1};\\
&M_{59} = \mathrm{e}^{\alpha\xi h_2};\quad M_{5(10)} = -\mathrm{e}^{-\alpha\xi h_2};\\
&M_{6(11)} = \mathrm{e}^{\alpha\xi h_2};\quad M_{6(12)} = -\mathrm{e}^{-\alpha\xi h_2};\\
&M_{71} = -e_{15}\mathrm{e}^{-\xi h_1};\quad M_{72} = e_{15}\mathrm{e}^{\xi h_1};\quad M_{75} = \varepsilon_{11}\mathrm{e}^{-\xi h_1};\quad M_{76} = -\varepsilon_{11}\mathrm{e}^{\xi h_1};\\
&M_{83} = -e_{15}\mathrm{e}^{-\xi h_1};\quad M_{84} = e_{15}\mathrm{e}^{\xi h_1};\quad M_{87} = \varepsilon_{11}\mathrm{e}^{-\xi h_1};\quad M_{88} = -\varepsilon_{11}\mathrm{e}^{\xi h_1};\\
&M_{91} = -e_{15};\quad M_{92} = e_{15};\quad M_{95} = \varepsilon_{11};\quad M_{96} = -\varepsilon_{11};\\
&M_{(10)3} = -e_{15};\quad M_{(10)4} = e_{15};\quad M_{(10)7} = \varepsilon_{11};\quad M_{(10)8} = -\varepsilon_{11};\\
&M_{(11)1} = -c_{44}^{(1)};\quad M_{(11)2} = c_{44}^{(1)};\quad M_{(11)5} = -e_{15};\quad M_{(11)6} = e_{15};\quad M_{(11)9} = \alpha c_{44}^{(2)};\quad M_{(11)10} = -\alpha c_{44}^{(2)};\\
&M_{(12)3} = -c_{44}^{(1)};\quad M_{(12)4} = c_{44}^{(1)};\quad M_{(12)7} = -e_{15};\quad M_{(12)8} = e_{15};\quad M_{(12)11} = \alpha c_{44}^{(2)};\quad M_{(12)12} = -\alpha c_{44}^{(2)}.
\end{aligned}
$$

References

1. Li, Y.D., Lee, K.Y.: Crack tip shielding and anti-shielding effects of the imperfect interface in a layered piezoelectric sensor. Int. J. Solid. Struct. **46**, 1736–1742 (2009)
2. Ru, C.: Electrode-ceramic interfacial cracks in piezoelectric multilayer materials. J. Appl. Mech. **67**, 255–261 (2000)
3. Govorukha, V.B., Loboda, V.V.: Contact zone models for an interface crack in a piezoelectric material. Acta Mech. **140**, 233–246 (2000)
4. Gu, B., Yu, S.W., Feng, X.Q.: Transient response of an interface crack between dissimilar piezoelectric layers under mechanical impacts. Int. J. Solid. Struct. **39**, 1743–1756 (2002)
5. Guo, X.H., Fang, D.N.: Simulation of interface cracking in piezoelectric layers. Int. J. Nonl. Sci. Num. Sim. **5**, 235–242 (2004)
6. Huang, G.L., Wang, X.D.: On the dynamic behaviour of interfacial cracks between a piezoelectric layer and an elastic substrate. Int. J. Fract. **141**, 63–73 (2006)
7. Li, Q., Chen, Y.H.: Analysis of a permeable interface crack in elastic dielectric/piezoelectric bimaterials. Acta Mech. Sin. **23**, 681–687 (2007)
8. Tian, W.Y., Rajapakse, R.K.N.D.: Fracture parameters of a penny-shaped crack at the interface of a piezoelectric bi-material system. Int. J. Fract. **141**, 37–48 (2006)
9. Li, Y.D., Lee, K.Y.: Fracture analysis on the arc-shaped interface in a layered cylindrical piezoelectric sensor polarized along its axis. Eng. Fract. Mech. **76**, 2065–2073 (2009)
10. Hausler, C., Jelitto, H., Neumeister, P. et al.: Interfacial fracture of piezoelectric multilayer actuators under mechanical and electrical loading. Int. J. Fract. **160**, 43–54 (2009)
11. Shin, J.W., Lee, Y.S.: A moving interface crack between two dissimilar functionally graded piezoelectric layers under electromechanical loading. Int. J. Solid. Struct. **47**, 2706–2713 (2010)
12. Loboda, V., Lapusta, Y., Sheveleva, A.: Limited permeable crack in an interlayer between piezoelectric materials with different zones of electrical saturation and mechanical yielding. Int. J. Solid. Struct. **47**, 1795–1806 (2010)
13. Natroshvili, D., Stratis, I.G., Zazashvili, S.: Interface crack problems for metallic-piezoelectric composite structures. Math. Meth. Appl. Sci. **33**, 539–562 (2010)
14. Kwon, J.H., Meguid, S.A.: Analysis of a central crack normal to a piezoelectric-orthotropic interface. Int. J. Solid. Struct. **39**, 841–860 (2002)
15. Kwon, S.M., Lee, K.Y.: Steady state crack propagation in a piezoelectric layer bonded between two orthotropic layers. Mech. Mater. **35**, 1077–1088 (2003)
16. Chen, Y.Z., Lin, X.Y., Wang, Z.X.: Antiplane elasticity crack problem for a strip of functionally graded materials with mixed boundary condition. Mech. Res. Commun. **37**, 50–53 (2010)
17. Li, Y.D., Lee, K.Y.: Collinear unequal crack series in magnetoelectroelastic materials: mode I case solved via new real fundamental solutions. Eng. Fract. Mech. **77**, 2772–2790 (2010)
18. Li, Y.D., Lee, K.Y.: Two collinear unequal cracks in a poled piezoelectric plane: Mode I case solved by a new approach of real fundamental solutions. Int. J. Fract. **165**, 47–60 (2010)
19. Liebowitz, H.: Fracture, An Advanced Treatise, Vol. 1 Microscopic and Macroscopic Fundamentals. Academic Press, New York (1968)
20. Yang, J.S.: An Introduction to The Theory of Piezoelectricity. Springer Science+Business Media, Inc., Boston (2005)
21. Zhong, X.C., Liu, F., Li, X.F.: Transient response of a magnetoelectroelastic solid with two collinear dielectric cracks under impacts. Int. J. Solid. Struct. **46**, 2950–2958 (2009)
22. Muskhelishvili, N.I.: Singular Integral Equations. Noordhoff, Groningen (1953)
23. Li, Y.D., Lee, K.Y.: Effects of magneto-electric loadings and piezomagnetic/piezoelectric stiffening on multiferroic interface fracture. Eng. Fract. Mech. **77**, 856–866 (2010)
24. Li, X.F., Lee, K.Y.: Closed-form solution for an orthotropic elastic strip with a crack perpendicular to the edges under arbitrary anti-plane shear. ZAMM. Zeit. Fur. Ang. Math. Mech. **89**, 370–382 (2009)
25. Matbuly, M.S., Nassar, M.: Analysis of multiple interfacial cracks in an orthotropic bi-material subjected to anti-plane shear loading. Eng. Fract. Mech. **76**, 1658–1666 (2009)
26. Duan, X.Y., Li, X.F.: An interfacially-cracked orthotropic rectangular bi-material subjected to antiplane shear loading. Appl. Math. Comp. **174**, 1060–1079 (2006)